Acoustic Emission Signal Detection in Drought-Stressed Trees: Beyond Counting Hits

Lidewei L. VERGEYNST *, Markus G. R. SAUSE **, Kathy STEPPE *
* Laboratory of Plant Ecology, Ghent University, Ghent, Belgium
** Experimental Physics II, University of Augsburg, Augsburg, Germany
Contact: Lidewei.Vergeynst@UGent.be

Abstract. Tree survival and fitness under changing environmental conditions with increasing drought stress is currently of high interest. When trees experience water shortage, the whole water transport system experiences strong tensions, which involves a risk of air-embolism formation in sap-conducting conduits. The phenomenon, in which air bubbles are formed in water under tension, is called 'cavitation' and has been associated with the generation of acoustic emission signals. Cavitation reduces the hydraulic conductivity of the water transport system and hampers the hydraulic performance, which may eventually lead to tree mortality. Although the significant role of cavitation during drought stress has been widely accepted, the processes of embolism formation and repair are still poorly understood. Detection of cavitation by acoustic emission might be a powerful non-destructive method to investigate this phenomenon. It has been shown that the cumulative number of hits gives an indication of the degree of cavitation, but quantification in the field is still doubtful with this empirical method. Moreover, it is still not known which processes are generating the acoustic emission signals in drought-stressed trees. We used broadband sensors to collect acoustic emission signals in dehydrating branches and examined the waveforms to get more insight into the source mechanisms of the respective acoustic emission signals. A pattern recognition algorithm was applied to identify natural clusters in the signals and the obtained waveform types were interpreted in terms of possible source mechanism and source location. Occurrence of cavitation was validated using X-ray computed tomography.

1. Introduction

A trees' vulnerability to cavitation is one of the major characteristics that will determine its chances of survival when droughts will occur more frequently. Cavitation is the formation of air bubbles in water under tension and leads to embolization of sap-conducting conduits in the wood. To compare the vulnerability to cavitation of different species, 'vulnerability curves' are constructed, which show the percentage of hydraulic conductivity loss as a function of xylem water potential. One of the many techniques to obtain vulnerability curves [1] uses the detection of acoustic emission (AE) signals to measure hydraulic conductivity loss during the dehydration of a cut branch segment [2–5]. When branch diameter shrinkage is simultaneously monitored during branch dehydration, three consecutive phases can be distinguished [4,5]. Firstly, release of water from living cells

results in a strong elastic shrinkage with few cavitation. When a certain threshold in water tension is reached, cavitation increases strongly, indicating the start of the second phase. At the end of the cavitation phase, all conduits are emptied and the sapwood has reached the so-called 'fibre saturation point'. The third phase consists of cell wall shrinkage, which also generates acoustic emissions of low amplitude [6], but this is no longer accompanied by large amounts of water release. When the elasticity of the wood is constant during dehydration, xylem tension (pressure water potential) can be derived from the continuously measured diameter shrinkage [5,7].

The acoustic method can be easily combined with continuous measurements of diameter variation and gravimetric water loss and because this method is non-destructive, also applications in the field are possible. However, the acoustic technique has not widely been used up to now because of the uncertainties related to the origin of acoustic emissions and its relationship with conductivity loss. Although AE activity is clearly related to embolism formation, a one-to-one relation [8] between the generation of AE signals and the number of embolized conduits has rarely been found. Experiments in which the number of AE signals exceeded the number of conduits [5,9] illustrate the need to understand the origin of AE signals from dehydrating wood.

Different AE source mechanisms typically result in distinct AE signals that could be identified based on the detected waveforms [10]. Therefore, we used a wideband point-contact sensor with very flat frequency response to collect waveforms from dehydrating grapevine branches (*Vitis vinifera* L. 'Johanniter') and searched for natural clusters of waveform types using an automated classification algorithm [11]. We chose grapevine branches because of the large vessels that could be easily distinguished on images obtained with X-ray micro-computed tomography. We used simultaneous visualisation of embolized conduits to validate the AE method and measured diameter shrinkage to be able to distinguish between the different phases of dehydration.

2. Material and methods

2.1 Dehydration experiments

Plant material was collected from 1-year-old grapevines (*Vitis vinifera* L. 'Johanniter') that were grown outdoors in 50-L containers. The grapevines were watered and the leaves of one branch of 73 cm length and 7.8 mm diameter were packed in an envelope of plastic and aluminium foil the evening before we harvested the branch. Early in the morning, before sunrise, the branch was excised under water and stripped of all leaves. The wounds and open ends were sealed with Parafilm and the branch was enclosed in a humid and light tight plastic bag for transportation to the scanner facility. We visualized the embolization of vessels during dehydration using the HECTOR (Masschaele et al. 2013), a custom-built micro-computed tomography (μCT) scanner at the Center for X-ray CT scanning of Ghent University (UGCT), Belgium. The branch was equipped with two broadband point contact sensors with a 20 dB internal preamplifier (KRNBB-PC sensor (Glaser and Nelson 1992) KRN Services, Richland, WA, USA), spaced 14 cm apart. The sensors are sensitive to out-of-plane displacements and have a very flat displacement response in the frequency range 20-1000 kHz. The AE signals, of 4096 samples length, were amplified by 35.6 dB and acquired at 5 MHz sample rate. The signals were processed by a digital filter with 20-1000 kHz band pass and all waveforms above the noise level of 28 dB were collected. Simultaneous with AE detection, we monitored the embolism status by scanning the branch continuously during two days of dehydration. We counted the embolized vessels visually and measured the average branch diameter (excluding the dead cortex) on 15 reconstructed

cross-sections throughout the dehydration period. Further details of the experiment are reported in Vergeynst et al. [5]. A similar dehydration experiment was conducted on a second branch (of about 7 mm diameter) with a dehydration time of 10 days, without μCT. On this branch, a linear variable displacement transducer (LVDT, DF/5.0, Solartron Mobrey, Brussels, Belgium) was installed on a small zone where the outer bark (dead cortex) was carefully removed and petroleum jelly was applied to prevent water loss through the bare xylem.

2.2 Waveform feature extraction and automated classification algorithm

In order to apply the classification algorithm we had to characterize the waveforms by a set of waveform features. We extracted a set of 8 features in the frequency domain: peak frequency (PF), frequency centroid (FC), weighted PF (geometric mean of PF and FC), the ratio PF over FC and the partial powers of the following frequency ranges: 0-100 kHz, 100-300 kHz, 300-550 kHz and 550-800 kHz. The features were chosen after screening the distributions of all available waveform features in NOESIS (Envirocoustics S.A., Athens, Greece) based on the presence of two or more local maxima in the distribution. A feature showing a unimodal distribution would have very little discriminating power. Before feature extraction, the onset of the signal was determined more precisely using a threshold of 23 dB. Feature extraction was conducted on the initial 50 μs after the time of arrival (250 samples) and frequencies below 50 kHz were filtered with an 8^{th} order Butterworth filter. We applied an automated classification algorithm as described by Sause et al. (2012) to identify natural clusters of acoustic emission signals. We screened the dataset for the presence of two to four clusters using each possible combination of four to eight signal features. Because of the enormous size of the datasets (more than 7.5 10^5 AE signals), we sampled 1200 AE signals for each of the 163 feature combinations.

3. Results

3.1 Automated classification algorithm

The optimal feature set detected by the classification algorithm consisted of PF, weighted PF, ratio FC over PF and partial power of the frequency interval 300-550 kHz (for 2-days dehydration experiment in scanner) and 550-800 kHz (for 10-days dehydration experiment). The cluster indices for the optimal clustering results are listed in Table 1. For visualization of the clustering results, we plotted the respective partial power against weighted PF (Fig. 1A, 1C). The automated classification algorithm resulted in two clusters for both dehydration experiments, partitioning the signals in a high frequency (blue) and low frequency (red) cluster. The corresponding normalized frequency distributions (average ± standard deviation) of both clusters are shown in Fig. 1B and 1D.

Table 1. Cluster indices for optimal clustering of AE signals during dehydration

Experiment	**Davies-Bouldin index**	**Tou-index**	**Rousseeuw's silhouette value**	**Pearson's Gamma statistic**
2-days dehydration in scanner	0.54	2.48	0.82	0.88
10-days dehydration	0.53	3.67	0.68	0.85

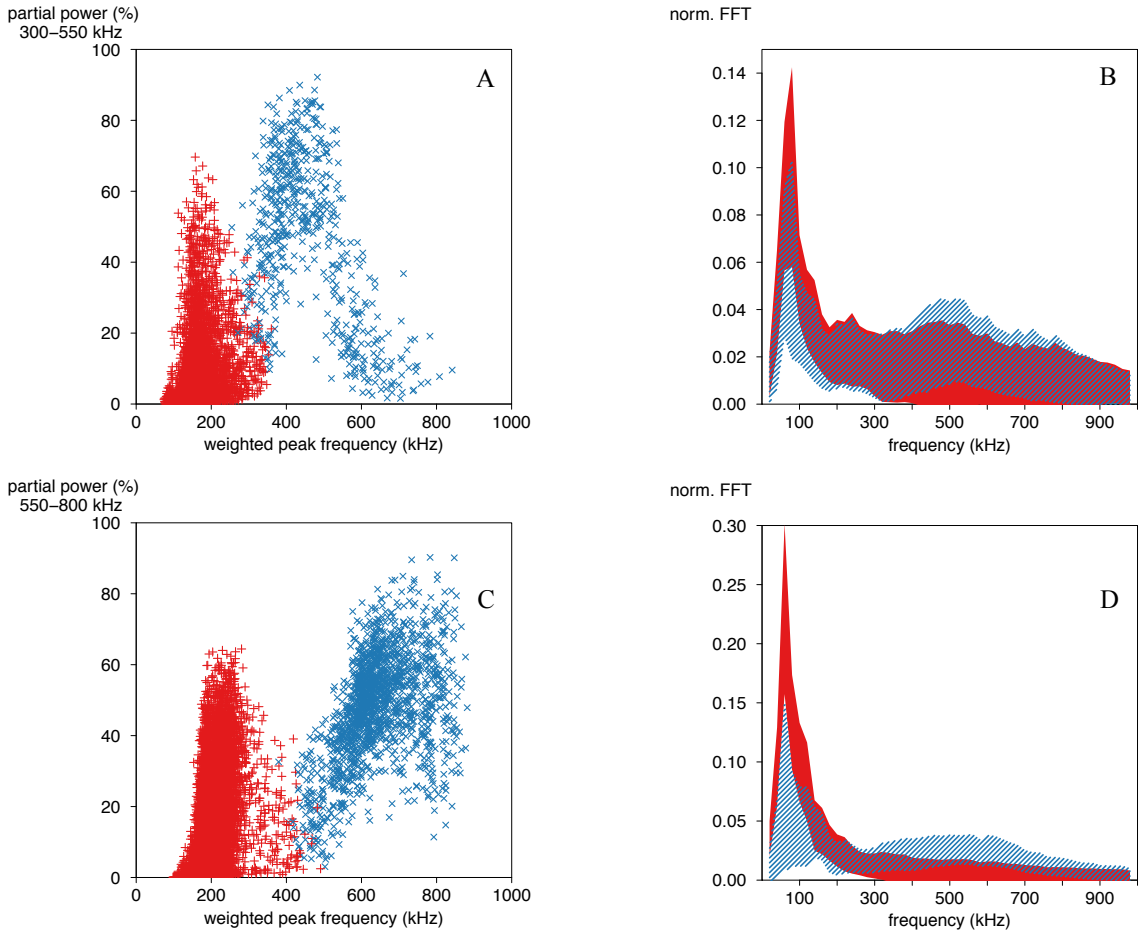

Fig. 1. Optimal k-means clustering of AE signals (left, sample of 10 000 AE signals) and average frequency distribution (± standard deviation) of both clusters (right) for the dehydration experiment of 2 days in the scanner (A, B) and of 10 days without scanner (C, D).

3.2 Vulnerability curves

We constructed the vulnerability curve (Fig. 2) as described by Vergeynst et al. [5] for both dehydration experiments, depicting cumulative AE signals (average of the two sensors) of both the low and high frequency clusters as a function of strain of the branch diameter ($\Delta d/d$). In Fig. 2A, we added the total number of embolized vessels since the start of the experiment, counted on µCT images. Note that the vulnerability curves in Fig. 2 are not complete. We distinguish only the first phase of elastic shrinkage and the beginning of the cavitation phase when the curve of embolized vessels became steeper (delimited by dashed line). The pattern of low frequency signals followed the pattern of visually observed embolized vessels, while the high frequency signals did not co-occur with embolization. The amount of high frequency signals is a factor of ten lower than the amount of low frequency signals. The initial part of the 10-days vulnerability curve (Fig. 2B) showed the same pattern for both clusters. However, at the end of the dehydration period, the number of AE signals increased exponentially (Fig. 3A). This exponential increase was associated with a strong peak in activity of the high frequency cluster (Fig. 3B). Both high and low frequency signals had a low amplitude during this high activity at the end of the dehydration period (Fig. 4).

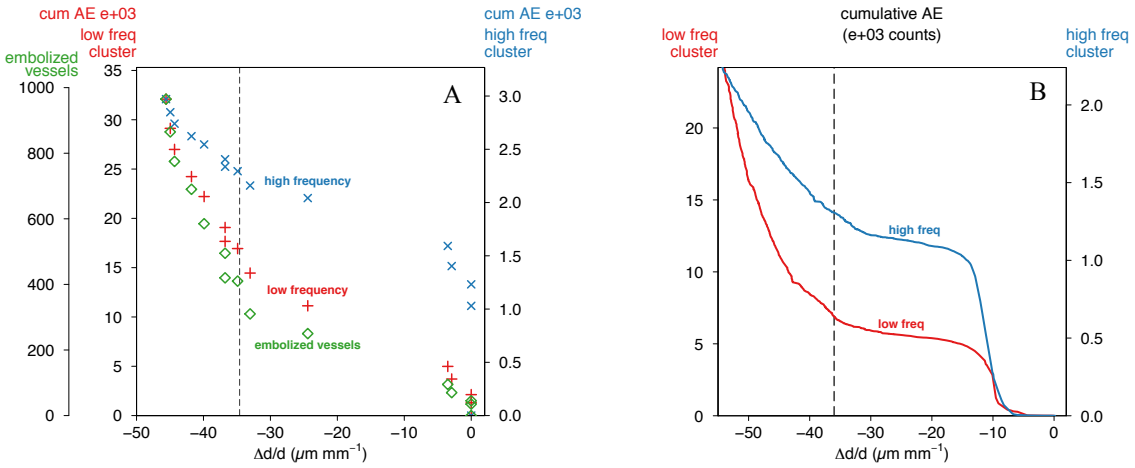

Fig. 2. First part of vulnerability curves depicting cumulative numbers of AE signals of low and high frequency clusters for the 2-days dehydration experiment, together with visually observed number of embolized vessels, plotted against strain of the branch diameter (A) and initial part of vulnerability curves for 10-days experiments (B), of which the complete curve is shown in Fig. 3A. A vertical dashed line indicates the transition between shrinkage phase and cavitation phase.

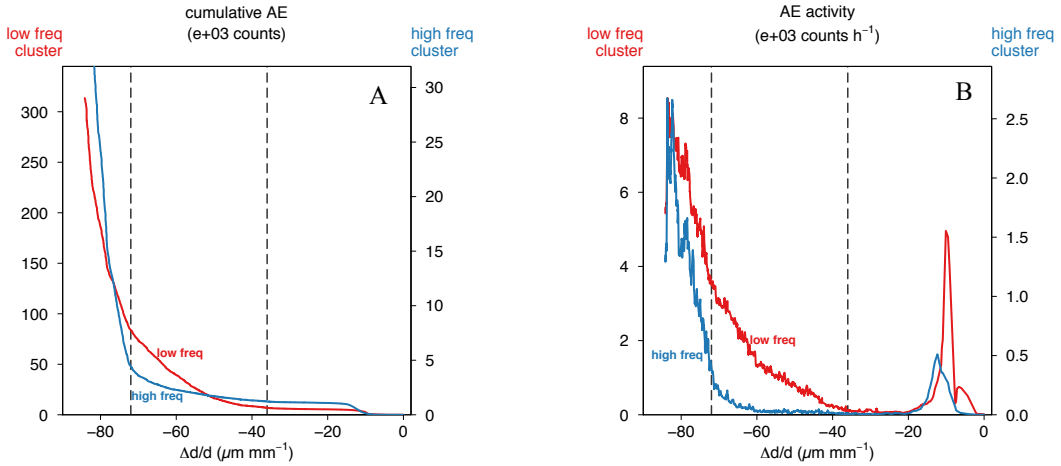

Fig. 3. Vulnerability curves of 10-days dehydration experiment (A) and AE activity per hour for both clusters plotted against branch diameter strain (B). Two vertical dashed lines delimit the cavitation phase.

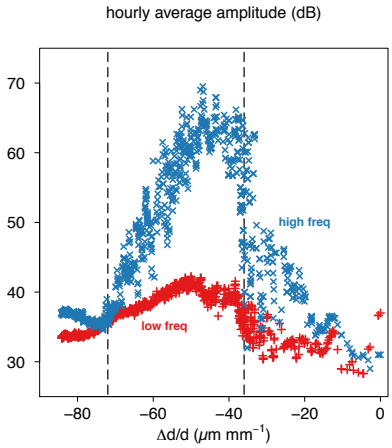

Fig. 4. Hourly average of signal amplitudes of both clusters during 10-days dehydration experiment as a function of branch diameter strain.

4. Discussion

4.1 Automated classification algorithm suggests two AE source types

The presence of two AE signal types in both dehydration experiments strongly suggests the activity of two different AE sources during dehydration of woody branches. We can distinguish between signals with mainly frequencies below 300 kHz, and signals with a stronger contribution of frequencies in the range 300-800 kHz (Fig. 1B, D). We refer to these clusters as the low and high frequency cluster. Comparing the distribution of weighted peak frequencies of both experiments (x-axis in Fig. 1A, C), we noticed that the clusters are located at somewhat higher frequencies for the second dehydration experiment (Fig. 1C) compared to the first one (Fig. 1A). The difference is probably due to the smaller diameter of the second branch, shifting the wave modes in a rod-like branch towards higher frequencies [12]. This explains why the automated classification algorithm selected the partial power 550-800 kHz to be more relevant for the second, smaller branch instead of the partial power 300-550 kHz for the first branch. The different behaviour of both clusters during the dehydration experiment (Fig. 2) confirmed that the clusters originated from at least two distinct source mechanisms.

4.2 Low frequency cluster co-occurs with embolization of grapevine vessels

During the 2-days dehydration experiment in the X-ray µCT scanner, we could verify which of the two clusters was related to the occurrence of embolisms. Although the total number of high frequency AE signals (3000) was closer to the total amount of embolized vessels (1000) than the total number of low frequency AE signals (35000), the pattern of the high frequency cluster did not follow the curve of vessel embolization (Fig. 2A). The pattern of the low frequency cluster, in contrast, nicely followed the pattern of visually observed embolization, suggesting an AE mechanism related to the invasion of air bubbles in the vessels. Low frequency signals have been related to capillary action in wood [16] and to the rearrangements of the air-water interfaces when water is displaced by air within a porous medium [17]. It has been shown that drainage of a porous medium involves rapid pore-scale meniscus displacements, called ‘Haines jumps’ [18]. A large portion of the energy change during a Haines jump is dissipated as elastic energy [19], resulting in acoustic emissions that could be measured in the frequency range 50-250 kHz [20], 10-30 kHz and below 3.75 kHz [17]. The invasion of one complete vessel with air probably involves multiple interfacial rearrangements, possibly explaining the large number of low frequency AE signals compared to the total number of embolized vessels (Fig. 2A).

4.3 Activity of high frequency cluster may indicate fibre saturation point

The high frequency cluster showed a high activity (Fig. 3B) of low amplitude AE signals (Fig. 4) at the end of the dehydration and a low activity (Fig. 3B) of high amplitude AE signals (Fig. 4) during the cavitation phase (delimited with dashed lines). AE signals with higher frequencies typically originate from faster mechanics at the AE origin [13,14]. In a study on cavitation in water under tension in a synthetic tree [15], they found a characteristic time of 0.1 µs for the formation of a bubble, which is a very fast process and probably results in high frequency signals. The large amplitude high frequency AE signals during vessel embolization could be suggestive of fast cavitation events in the sap under tension. However, the high activity of this cluster after the cavitation phase suggests microscopic fracture mechanisms rather than cavitation. Because of uneven water loss over the branch cross section, large tensions develop inside the wood during dehydration [21], which may result in micro-fractures in or between the cell walls. This might be another source of strong high frequency signals during the cavitation phase. When all vessels are emptied (so-called fibre saturation point), the cell walls start to shrink, which may cause many acoustic emissions due to fissures in or between the cell walls, resulting in the final high frequency AE activity peak. As the water content is much more in equilibrium at that point, tensions are reduced and the AE signals are of lower amplitude. It is remarkable that the embolization at the very beginning of dehydration (above -10 µm mm^{-1} in Fig. 2A) is also accompanied by a peak in high frequency signals. We assume that these signals are caused by strong dehydration dynamics at the open branch ends.

4.4 Detection of two clusters beneficial for construction of vulnerability curves

The vulnerability curves as obtained with 150 kHz resonance sensors [5] levelled off near the end of dehydration, when all vessels were emptied. We defined the point of 100% loss of hydraulic conductivity at the deflection point of this curve. However, the vulnerability curve for the low frequency cluster, which was related to embolization, showed an increased steepness after the cavitation phase when using broadband sensors (Fig. 3A). It is possible that signals from the high frequency cluster were altered by propagation along the branch and ended up in the low frequency cluster due to stronger attenuation of the high frequencies. Further experiments will be conducted to proof that the final activity peak of the high frequency cluster indicates the point when fibre saturation is reached and thus 100% loss of hydraulic conductivity. The use of the broadband sensor would be favourable to construct vulnerability curves when the high frequency cluster provides a solid determination of the endpoint.

5. Conclusion

The use of broadband point contact sensors during dehydration of woody branches revealed two types of acoustic emission sources. The low frequency signals are related to the formation of embolisms and could be used to quantify relative loss in hydraulic conductivity. Wood fractures during dehydration probably result in high frequency signals and a high activity of this cluster may indicate the point when fibre saturation is reached. The distinction between both types of AE sources could improve the reliability of the acoustic method for construction of vulnerability curves.

References

[1] Cochard, H., Badel, E., Herbette, S., Delzon, S., Choat, B., and Jansen, S., 2013, "Methods for measuring plant vulnerability to cavitation: a critical review," J. Exp. Bot., 64, pp. 4779–4791.

[2] Lo Gullo, M. A., and Salleo, S., 1993, "Different vulnerabilities of Quercus ilex L. to freeze- and summer drought-induced xylem embolism: an ecological interpretation," Plant Cell Environ., 16, pp. 511–519.

[3] Cochard, H., 1992, "Vulnerability of several conifers to air embolism," Tree Physiol., 11, pp. 73–83.

[4] Vergeynst, L. L., Bogaerts, J., Baert, A., Kips, L., and Steppe, K., 2013, "New type of vulnerability curve gives insight in the hydraulic capacitance and conductivity of the xylem," Acta Hort., 991, pp. 341–347.

[5] Vergeynst, L. L., Dierick, M., Bogaerts, J., Cnudde, V., and Steppe, K., in press, "Cavitation: a blessing in disguise? New method to establish vulnerability curves and assess hydraulic capacitance of woody tissues," Tree Physiol.

[6] Wolkerstorfer, S. V., Rosner, S., and Hietz, P., 2012, "An improved method and data analysis for ultrasound acoustic emissions and xylem vulnerability in conifer wood," Physiol. Plant., 146, pp. 184–191.

[7] Alméras, T., Yoshida, M., and Okuyama, T., 2006, "Strains inside xylem and inner bark of a stem submitted to a change in hydrostatic pressure," Trees, 20, pp. 460–467.

[8] Tyree, M. T., Dixon, M. A., Tyree, E. L., and Johnson, R., 1984, "Ultrasonic acoustic emissions from the sapwood of cedar and hemlock: an examination of three hypotheses regarding cavitations," Plant Physiol., 75, pp. 988–992.

[9] Rosner, S., Klein, A., Wimmer, R., and Karlsson, B., 2006, "Extraction of features from ultrasound acoustic emissions: a tool to assess the hydraulic vulnerability of Norway spruce trunkwood?" New Phytol., 171, pp. 105–116.

[10] Sause, M. G. R., Müller, T., Horoschenkoff, A., and Horn, S., 2012, "Quantification of failure mechanisms in mode-I loading of fiber reinforced plastics utilizing acoustic emission analysis," Compos. Sci. Technol., 72, pp. 167–174.

[11] Sause, M. G. R., Gribov, A., Unwin, A. R., and Horn, S., 2012, "Pattern recognition approach to identify natural clusters of acoustic emission signals," Pattern Recognit. Lett., 33, pp. 17–23.

[12] Vergeynst, L. L., Sause, M. G. R., Hamstad, M. A., and Steppe, K., unpublished, "Deciphering acoustic emission signals in drought stressed branches using broadband sensors and finite element modelling."

[13] Scruby, C. B., 1985, "Quantitative acoustic emission techniques," Nondestructive testing Vol. 8, Academic Press, Inc., London, pp. 141–208.

[14] Hamstad, M. A., 2010, "On lamb modes as a function of acoustic emission source rise time," J. Acoust. Emiss., 28, pp. 41–47.

[15] Vincent, O., Marmottant, P., Quinto-Su, P. A., and Ohl, C.-D., 2012, "Birth and growth of cavitation bubbles within water under tension confined in a simple synthetic tree," Phys. Rev. Lett., 108, 184502.

[16] Rosner, S., 2012, "Waveform features of acoustic emission provide information about reversible and irreversible processes during spruce sapwood drying," BioResources, 7, pp. 1253–1263.

[17] DiCarlo, D. A., 2003, "Acoustic measurements of pore-scale displacements," Geophys. Res. Lett., 30, 1901.

[18] Haines, W. B., 1930, "Studies in the physical properties of soil. V. The hysteresis effect in capillary properties, and the modes of moisture distribution associated therewith," J. Agric. Sci., 20, pp. 97–116.

[19] Berg, S., Ott, H., Klapp, S. a, Schwing, A., Neiteler, R., Brussee, N., Makurat, A., Leu, L., Enzmann, F., Schwarz, J.-O., Kersten, M., Irvine, S., and Stampanoni, M., 2013, "Real-time 3D imaging of Haines jumps in porous media flow.," PNAS, 110, pp. 3755–3759.

[20] Chotard, T., Smith, A., and Quet, A., 2007, "Characterisation of liquid transfer processes and water adsorption mechanism on a porous ceramic by acoustic emission means," J. Eur. Ceram. Soc., 27, pp. 457–462.

[21] Jakieła, S., Bratasz, Ł., and Kozłowski, R., 2007, "Numerical modelling of moisture movement and related stress field in lime wood subjected to changing climate conditions," Wood Sci. Technol., 42, pp. 21–37.